





Modification Design and Process of Pipeline to Reduce Erosion Rate and Deposited

Haider Sami Salman¹, Mustafa M. Mansour^{2*}, Alaa M. Lafta², Ahmed J. Shkarah²

¹ Department of Petroleum and Gas Engineering, College of Engineering, University of Thi-Qar, Thi-Qar 64001, Iraq

² Department of Mechanical Engineering, College of Engineering, University of Thi-Qar, Thi-Qar 64001, Iraq

Corresponding Author Email: mustafa.muhammedali@utq.edu.iq

Copyright: ©2024 The authors. This article is published by IETA and is licensed under the CC BY 4.0 license (<http://creativecommons.org/licenses/by/4.0/>).

<https://doi.org/10.18280/ijcmem.120206>

ABSTRACT

Received: 16 January 2024

Revised: 16 April 2024

Accepted: 10 May 2024

Available online: 30 June 2024

Keywords:

crude oil, particle-laden flow, CFD, erosion, solid rotator fin, elbow

In the gas and industry, erosion that is brought on by particles in pipe bends is a severe issue that can lead to failure or equipment malfunction. The computational fluid dynamics (CFD) approach is primarily utilized in the presented study in order to investigate the erosion distributions as well as particle trajectories in pipe bends under various influencing conditions. Throughout upstream petroleum production activities, crude oil as well as eroded sand from formation zones is frequently transported together via pipes up to flow stations and between flow stations and pipe. The rotator fin is propelled by flow momentum in the stream-lines which are particle-laden flow pipe walls, particularly at the elbows, causing erosive damages, which could result in costly and disastrous system failure. Thus, calculating the erosion rate while the system is operating is essential to predict failures and preventing them. Of all fittings used in the piping systems, the elbows are the most prone to experience erosions brought on by oil-carried rotator fins that veer off course and strike the walls as they pass through the bent portions of elbows. The numerical simulation-based erosion prediction model was used in order to calculate relative erosion severity so as to lessen erosive damage caused through the solid rotator fin. Physical features such as particle tracking, flow turbulence, and erosion simulation were merged in this work to create the potentials needed to fully represent the present issue. The computational simulation related to crude oil flow offers comprehensive insights, but it also allows for the avoidance of significant expenses and laborious attempts associated with conventional experiments. The new analysis provides invaluable physical information that may be utilized to assess oil recovery and employ the model as an alternate particle-laden flow management tool. Additionally, it might pinpoint limiting processes and elements; develop a computer-aided tool to optimize and design future pipe systems for increasing their lifetime by enhancing their erosion resistance, which would undoubtedly save a significant amount of cost and time.

1. INTRODUCTION

The leakage regarding crude oil from natural deposits is one of the main approaches it harms the environment today [1]. Particle-laden flow from reservoirs is frequently moved up to well heads and from well heads to upstream flow stations throughout upstream petroleum production techniques. Because of the pressure reduction, the entrained particle-laden flow could deposit on elbow pipe's walls, leading to issues with erosive wear and eventually crude oil leakage (Figure 1). Particle-laden flow causes substantial erosive damages to pipe walls through being carried by the flow momentum in streamlines which strike them, especially at elbows. This could result in a costly and disastrous system failure [2]. Because of its critical function in oil industry and its practical applications regarding material erosion, pipe elbows erosion generated by particle-laden flow rotator fin has lately attracted a lot of attention. In order to handle the issues regarding erosion brought on by solid rotator fins carried with fluid flow,

both materials engineering and fluid dynamics are necessary [3-5]. Thus, it has been considered essential to predict any potential failure in advance and, through calculating the erosion rate while the system is operating, avoid it.



Figure 1. Piping systems in the oil sector demonstrate how elbows erode

The development related to anti-erosion elbows was

hampered by lack of effective testing equipment to assess the rate of erosion brought on by flow through piping systems. Particle-laden flow erosion is too complex because it takes into account a variety of structural and hydrodynamic elements, such as the properties regarding the oil as well as its flow rate, the materials utilized for fittings, the flow rate of particle-laden flow as well as its rotator fin features, and the geometrical characteristics regarding elbows, such as shape and size, that could either negatively or positively affect the erosion's severity. Because of this, it has become quite interesting to manipulate such design elements at the same time in order to lessen the detrimental impacts of erosion caused by solid rotator fins.

Thus, a variety of predicting techniques have been created to reduce the erosion's effects. One of them was proven to be extremely applicable and effective to the overly complex engineering applications (CFD-based erosion simulation) [6, 7]. For predicting the rates of erosion, a 3D CFD model which specifies the turbulent transport regarding sand as well as crude oil through elbows was constructed in this work. Flow turbulence, particle tracking, and erosion rate simulations have all been incorporated.

Objectives: Investigated the influence of particle-laden on flow field characteristics, particle motion trajectories, and erosion rates in pipeline elbows

Methodology: The method and device proposed in the paper can accurately determine the maximum erosion rate of an L-shaped pipeline, improving the accuracy of the acquired erosion rate

The key findings: The analyzed area in present simulation is limited to the 3D part of the elbow as visualization of the entire elbow modeled numerically requires a high-end and expensive computer hardware and excessively large simulation time as depicted in the Figure 2.

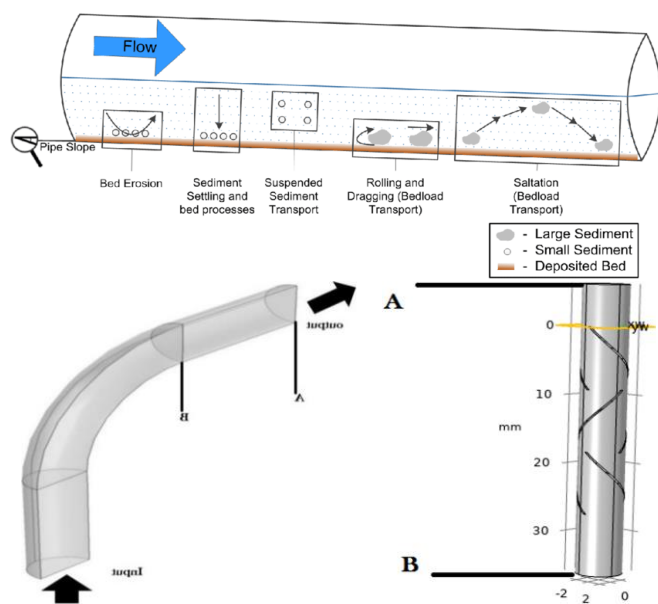


Figure 2. 3D computational domain

2. CFD MODELING

The particle tracking, continuous phase flow field simulation, and erosion calculations are the three primary steps in the CFD-based erosion modeling process. Navier-Stokes equations are used for solving the gas through treating it as

continuous phase. Newton's second law is applied to the particles as discrete phase and provides a solution. Two-way coupling has been applied between discrete and continuous phases.

The article estimates the maximum erosion rate in gas-solid two-phase flow pipelines taking into account factors such as pressure, solid content, throttle valve opening, and pipe diameter will help to reduce uncertainties about erosion rate prediction. A finite element model of gas-solid two-phase flow pipeline erosion considering not only field data was established and validated by running the model, and a general erosion rate prediction formula was deduced using the wall thickness detected in the field.

An increase in the erosion rate in a pipeline has been observed by these factors such as solid particle size, inlet velocity, with higher velocities and larger particles leading to an accelerated erosion process. a parametric study using detailed parameters such as the location of fin, flow rate, fluid viscosity and density of the solid particle was conducted to determine the key parameter that has the higher potential to erode a pipeline.

2.1 Computational domain

The relationship between the elasticity of the surface and the movement of the particles is also not regarded as erosion time advances, thereby making its erosion characteristics non-time reliant. However, the Erosion-coupled dynamic grid is a combination of two models, namely the erosion rate solver model. Regarding the dynamic, as the erosion time increases the H/W and S/D spacers shape becomes more complex.

The helical with pipeline erosion rate determining method and apparatus in the paper provide a formula to accurately determine the maximum erosion rate of the pipeline. In this article, an helical with pipeline erosion rate determining method and apparatus for determining the maximum erosion rate of a pipeline has been presented, which is based on the open degree of a flow controlling valve on the pipeline and the start pressure of the pipeline.

CFD models predict erosion rates more accurately at higher velocities compared to experimental data. The technical field of erosion corrosion protection of an oil-gas mixture transportation pipeline, in particular to an equal-flow multilevel flow rate mixture pipeline erosion field test apparatus, was addressed.

2.2 Modeling equations

Turbulence flow model

A fluid with constant density that is Newtonian and incompressible is taken into consideration. Continuity equations and momentum conservation are expressed in RANS forms as [8]:

$$\begin{aligned} \rho \frac{\partial U}{\partial t} + \rho U \cdot \nabla U + \nabla \cdot (\overline{\rho u' \otimes u'}) \\ = -\nabla P + \nabla \cdot \mu (\nabla U + (\nabla U)^T) + F \\ \rho \nabla \cdot U = 0 \end{aligned} \quad (1)$$

where, U denotes average velocity, whereas \otimes represents outer vector product. Since its more accurate compared to k- ϵ model for flows that involve strong stream-line curvature, k- ω model has been carefully selected in the study [8]. The formulation regarding this turbulence model is:

$$\rho \frac{\partial k}{\partial t} + \rho u \cdot \nabla k = \left(\frac{P_k - \rho \beta^* k \omega +}{\nabla \cdot ((\mu + \sigma^* \mu_T) \nabla k)} \right) \quad (2)$$

$$\rho \frac{\partial \omega}{\partial t} + \rho u \cdot \nabla \omega = \left(\frac{\alpha \frac{\omega}{k} P_k - \rho \beta \omega^2 +}{\nabla \cdot ((\mu + \sigma \mu_T) \nabla \omega)} \right) \quad (3)$$

where,

$$\mu_T = \rho \frac{k}{\omega}, \alpha = \frac{13}{25}, \beta = \beta_o f_\beta, \beta^* = \beta_o^* f_\beta \quad (4)$$

$$\sigma = \frac{1}{2}, \sigma^* = \frac{1}{2} \quad (5)$$

$$\beta_o = \frac{13}{125}, f_\beta = \frac{1 + 70X_\omega}{1 + 80X_\omega}, X_\omega = \left| \frac{\Omega_{ij} \Omega_{jk} S_{ki}}{(\beta_o^* \omega)^3} \right|$$

$$\beta_o^* = \frac{9}{100} f_\beta^* = \begin{cases} 1 + 680X_k^2 \\ 1 + 400X_k^2 \end{cases} \quad (6)$$

$$X_k = \frac{1}{\omega^3} (\nabla k \cdot \nabla \omega) \quad (7)$$

$$\begin{cases} X_k \leq 0 \\ X_k > 0 \end{cases}$$

where, ω_{ij} denotes the mean tensor of rotation rate [9].

$$\Omega_{ij} = \frac{1}{2} \left(\frac{\partial u_i}{\partial x_j} - \frac{\partial u_j}{\partial x_i} \right) \quad (8)$$

where, S_{ij} represents the mean strain rate tensor [10].

$$S_{ij} = \frac{1}{2} \left(\frac{\partial u_i}{\partial x_j} + \frac{\partial u_j}{\partial x_i} \right) \quad (9)$$

$$P_k = \mu_T \left(\nabla u : (\nabla u + (\nabla u)^T) - \frac{2}{3} \rho k \nabla \cdot u \right) - \frac{2}{3} \rho k \nabla \cdot u \quad (10)$$

3. PARTICLE MOTIONS IN THE FLUID MODEL

Newton's second law states that particle momentum could be expressed in the following form [8].

$$\frac{d}{dt} (m_p V) = F_D + F_g + F_{ext} \quad (11)$$

where, m_p denotes particle mass in kilograms, v .

$$F_g = m_p g \frac{(\rho_p - \rho)}{\rho_p} \quad (12)$$

where, ρ_p denotes particle density in kg/m^3 , g represents direction of gravitation, and ρ represents surrounding fluid density in kg/m^3 .

4. MODELS OF EROSION

Erosion feature figures out erosive wear rate or total mass removed per area as a result of a rotator fin's impact at a

boundary. The three models listed below were created [4-7].

4.1 DNV erosion model

To predict erosion of the plugged tees, straight pipes, reducers, elbows, and welded joints, Det Norske Veritas (DNV) created an erosion model in 2007. Different experimental data and numerically projected findings were used to construct this model. The model is demonstrated by:

$$\mu_T = ER = CF(\theta) V_p^n \quad (13)$$

$$F(\theta) = \sum_{i=1}^8 (-1)^{i+1} A_i \theta^i$$

where, ER stands for target's rate of erosion and is specified as mass loss regarding the wall per unit of time and area. Erosion rate (ER) can be ultimately defined in this work as rate of penetration, calculated through dividing the rate of erosion by pipe wall material density. The function of impact angle can be denoted by $F(\theta)$, the constant $C=2 \times 10^{-9}$ for the steel pipes, and n represents the exponent of velocity, for steel pipes, $n=2.60$. Table 1 lists the values of A_i .

Table 1. Base case and Eyrer's experimental flow conditions used in the model [11]

Name	Values	Parameter	Values
Fluid	Air	Temperature	298.15 K
Particle diameter	100 μm	Carrier fluid	Crudo oil
Particle density	2650 kg/m^3	Nominal velocity	0.3 m/sec
Velocity	25.24 m/s	fin diameter	2 cm
Particle mass flow rate	0.0286 kg/s	Oil viscosity	8 mPa.s
Brinell hardness (BH) of pipe wall	120	Oil density	850 kg/m^3
Density of the pipe material	7800 kg/m^3	Pipe diameter	0.75 m
		Pipe material	iron

4.2 E/CRC model of erosion

Univ. of Tulsa's Erosion/Corrosion Research Center (E/CRC) came up with this model [11]. This model was developed for the prediction of carbon steel erosion on the dry or wet surfaces. It depends on numerous direct impact experimentations for various particle shapes and impact angles. Zhang et al. [4] provided the equations below:

$$ER = C(BH)^{-0.59} F_s u_p^n F(\theta) \quad (14)$$

$$F(\theta) = \sum_{i=1}^5 R_i \theta^i$$

where, $C = 2.17 \times 10^{-7}$ for the carbon steel, F_s represents factor of particle sharpness, BH represents Brinell hardness of target material, $F_s = 1$ for the sharp sand particles, $n = 2.41$, 0.53 for semi-rounded particles of the sand, and 0.20 for rounded particles of sand. Table 1 shows R_i values.

4.3 Neilson and Gilchrist erosion model

Depending on their experimental findings, Bikbaev et al. [12] created an erosion model. For the prediction of erosions rate at large and small impact angles, they developed two equations. The first term on right-hand side of equations below reflects erosion brought on by the cutting, while 2nd term denotes erosion brought on by the deformation.

$$ER = \frac{u_p^2 \cos^2 \theta \sin \frac{\pi \theta}{2 \theta_0}}{2 \varepsilon_C} + \frac{u_p^2 \sin^2 \theta}{2 \varepsilon_D} \theta < \theta_0 \quad (15)$$

$$ER = \frac{u_p^2 \cos^2 \theta}{2 \varepsilon_C} + \frac{u_p^2 \sin^2 \theta}{2 \varepsilon_D} \theta > \theta_0 \quad (16)$$

where, θ_0 represents the angle of transition, which has generally been set as $\pi/4$, ε_C represents cutting coefficient [13], set to the value of 3.332×10^7 , ε_D represents the coefficient of deformation, which has been set to the value of 7.742×10^7 .

4.4 Oka et al. erosion model

More influencing elements than the three models mentioned above were considered [14], who presented the following model:

$$ER = 1.0 \times 10^{-9} \rho_w k F(\theta) (Hv)^{k_1} \left(\frac{u_p}{V'}\right)^{k_2} \left(\frac{d_p}{d'}\right)^{k_3} \quad (17)$$

$$F(\theta) = (\sin \theta)^{n_1} [1 + Hv(1 - \sin \theta)]^{n_2} \quad (18)$$

where, ρ_w represent density regarding target material, d_p represent particle diameter, d' represents reference diameter, Hv represent Vickers hardness related to target material, V' represents impact velocity related to reference particle [14]. Table 1 lists the followings: $k, k_1, k_2, k_3, n_1, n_2, d$ and V' .

4.5 Duarte et al. erosion model

A model for prediction of the rate of slurry erosion in different geometries was put up by Duarte et al. [15]. The model was created using CFD simulations as well as experimental data from material erosion.

$$ER = A(BH)^{-0.59} F_s u_p^n F(\theta) \quad (19)$$

$$F(\theta) = a \theta^2 + b \theta \quad \theta \leq \theta_0 \quad (20)$$

$$F(\theta) = x \cos^2 \theta \sin(w\theta) + y \sin^2 \theta + z \quad \theta > \theta_0$$

where, A, B, C, D, E and F are all of the coefficients of correlation that have been listed in Table 1.

4.6 Hashish erosion model

A model of erosion depending on summation of the cutting and deformation erosion was created by the study [16], the model is presented:

$$ER = \frac{100}{2\sqrt{29}} d_p^3 \left(u_p \sqrt{\frac{\rho_p}{3\sigma R_f^{0.6}}} \right)^n \sin 2\theta \sqrt{\sin \theta} \quad (21)$$

where, ρ_p represents solid particle density, $n = 2.54$, σ represents plastic flow stress, R_f represents roundness factor.

4.7 Huang et al. erosion model

A single particle erosion model was put forth by Huang et al. [17]. Deformation damage and cutting are considered in this model.

$$ER = K \rho_p^{0.1875} d_p^{0.5} u_p^{2.375} (\cos \theta)^2 (\sin \theta)^{0.375} \quad (22)$$

where, K represents a constant is dependent upon the characteristic of target material. The following definitions apply to parameters: the idealized fraction of rotator fin cutting is denoted by c (dimensionless).

M [Kg] represents eroding rotator fin total mass.

U [m/s] represents incident particle velocity magnitude.

m [kg] represents mass regarding individual particle hitting surface.

p [Pa] represents material Vickers hardness.

r [m] represents mean particle radius.

I [kg-m²] represents inertia moment of individual particle about its mass center. For isotropic sphere, $I = 2mr^2/5$ [18].

α [rad] Represents incidence angle, with $\alpha = 0$ tangent to surface and $\alpha = \pi/2$ normal to surface.

P Represents a dimensionless parameter, which has been specified as $P = K/(1 + mr^2/I)$ [19], in which K (dimensionless) is ratio of the horizontal and vertical forces acting on particle.

With regard to Finnie model, it is presumable that rotator fins use an idealized cutting process for removing the mass from the surface. It is advised for modeling ductile material erosion by rotator fins at short angles of incidence because it doesn't predict any erosive wear by rotator fin at normal incidence to the surface.

5. E/CRC MODEL

The mass lost by surface divided by the mass of rotator fin that was incident defines the erosion rate according to the E/CRC model:

$$E = CF_s (BH)^{-0.59} \left(\frac{v}{1 [m/sec]} \right)^n F(\alpha) \quad (23)$$

$$F(\alpha) = \left(\frac{5.40\alpha - 10.11\alpha^2 + 10.93\alpha^3 -}{6.33\alpha^4 + 1.42\alpha^5} \right) \quad (24)$$

where, F_s represents a dimensionless particle shape coefficient, C represents a dimensionless coefficient of the model and BH represents a dimensionless measure of wall material's Brinell hardness. In radians, the angle of incidence is expressed [20].

6. EROSION RATE (DNV) MODEL

According to DNV model, erosion rate is expressed as the mass of incident rotator fin divided by the mass lost by surface [21].

$$E = K \left(\frac{v}{1 [m/s]} \right)^{-n} F(\alpha) \quad (25)$$

$$F(\alpha) = \left(\frac{9.370\alpha - 42.295\alpha^2 + 110.864\alpha^3 -}{98.398\alpha^6 + 31.211\alpha^7 - 4.170\alpha^8} \right)$$

where, n and K are constants depending on surface material.

7. THE USED GRID

The governing equations had been discretized with the use of finite-volume approach, and then they were solved utilizing

multi-physics capable commercial CFD tool COMSOL v6.1. To verify that the solutions that have been obtained utilizing the chosen mesh are independent of grid size, grid sensitivity was done. It was determined that the chosen grid's total of 8908 boundary elements, 44772 domain elements, and 590 edge elements provided enough spatial resolution (Figure 3). The coupled equations were iteratively solved, and an error limit of 1.0×10^{-6} was deemed adequate to obtain convergence of the result. In the case when the relative error between two successive iterations was less than in each field, the solution was deemed to be convergent. This study's erosion prediction approach, which includes 3 main steps—flow modeling, particle tracking, and erosion predictions—is a complete procedure depending on a 3D CFD method. Table 1 lists flow's initial and boundary conditions [22].

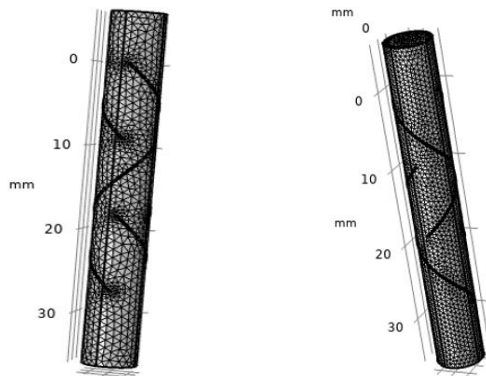


Figure 3. Domain's three-dimensional computational mesh

The 3-D computational mesh that has been utilized in the simulation. Meshing includes 2 parts: the 1st one is surface meshing and the 2nd one is the volume meshing. Surface mesh has been generated carefully as a result of its significant impact on the quality of flow.

8. RESULTS

Pollutant particle trajectories were traced and assessed, and erosion on pipe elbows was compared across different input velocities. In this study, the elbow's inflow velocity serves as the independent variable for erosion modeling, with values ranging from 2m/s to 20m/s (Figure 4). The erosion rate at the elbow is calculated using the erosion rate change trend chart. The rate of erosion increases as the input velocity increases. When the inflow velocity ranges from 2 to 10 meters per second, the erosion rate at the pipeline's elbow steadily increases however, when the input velocity ranges between 10 and 20 m/s, the erosion velocity increases significantly. In this model, 10m/s is the tipping point for erosion rate rise. The fluid transports pollution particles to the pipeline. In the straight pipe section, particles are evenly dispersed in both the continuous and scattered phases. At this point, the fluid is steady, and pollution particles have a greater incidence angle. At the pipe bend, the outside of the pipe generates resistance to the fluid's flow direction, forcing the flow to alter. The number of pollution particles in the elbow of the acute Angle is reduced, resulting in pipeline degradation, as seen in Figure 5.

Figure 6 displays crude oil's passing through pipe elbow's velocity distribution. The figure demonstrates the existence of a zone of separation following the curve. A comparable

distribution of pressure in pipe elbow is shown in Figure 7. Figure 8 depicts sand transport directions' visualizations through elbow of the pipe. The only rotator fins that made contact with pipe bend surfaces are visible since all other rotator fins that pass through pipe bend without touching walls were hidden. The acute incidence angle, expressed in degrees and measured from the surface normal, determines the color expression. It is evident that the rotator fin merely makes grazing contact with the surface. The erosive wear rate on pipe elbow surface of contaminated crude oil with particle-laden flow is simulated using three distinct erosion models. Figures 7-9 depict, respectively, Finnie, DNV, and E/CRC erosion. Figure 10 provides a good example of erosion occurring in a pipe elbow throughout flow of contaminated crude oil with a particle-laden flow rotator fin.

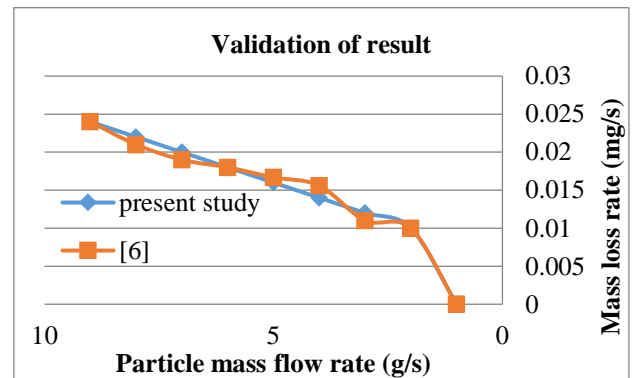


Figure 4. Comprehensive present model and results to estimate erosion parameter [6]

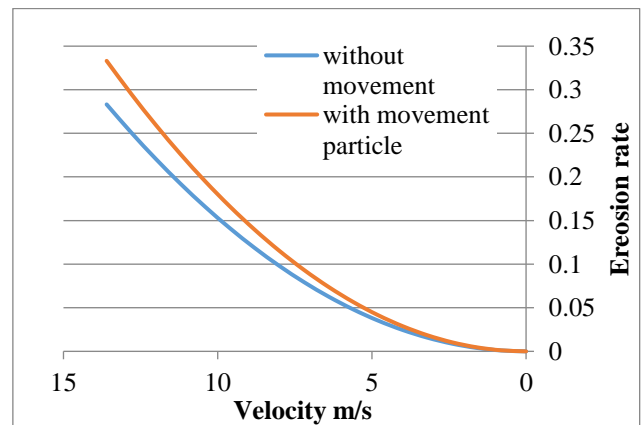


Figure 5. Influence of the movement particle on the erosion-related variables

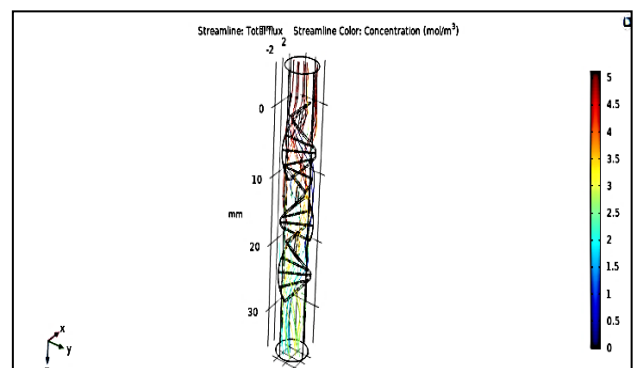


Figure 6. Velocity streamlines [m/sec] in pipe elbow

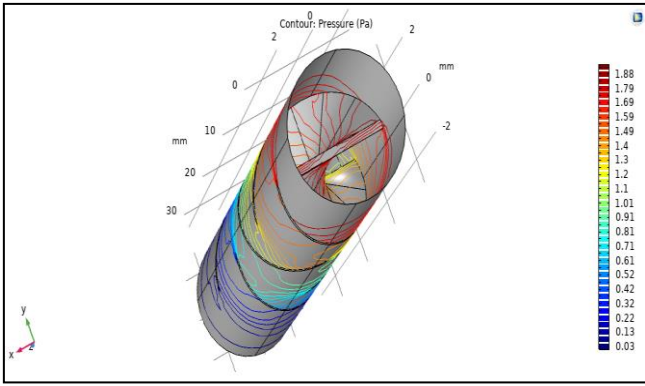


Figure 7. Pressure [Pa] in pipe elbow

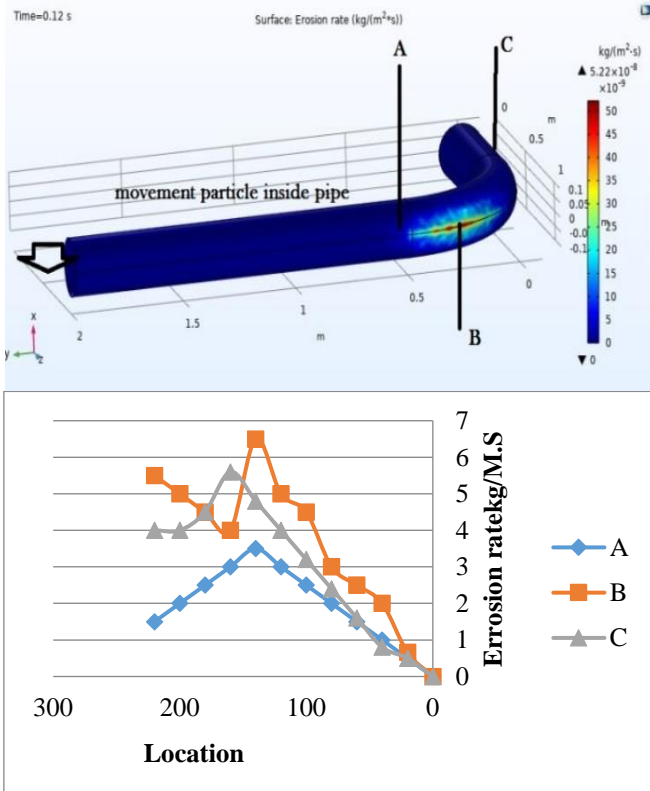


Figure 8. Visualizations of directions transport through pipe elbow. The color expression is acute incidence angle [degree], which has been measured from surface normal

The rise of the inflow fluid velocity sets the spatial distribution of particles, which also causes the effect of friction between the particles and the inner liner. The maximum erosion spot migrates from the outside the barrier to the inner side at 6 m/s. This shows the maximum erosion rate is very smooth along the inner wall at velocities 5 m/s, 6 m/s, and 7 m/s. The inner surfaces' peak value coordinates are approximately 70° for the outer wall. Data on fluid velocity, solid particle size, concentration, and spatial distribution of particles influence particle impact behavior. Particle image velocimetry (PIV) technique is employed to measure velocities in the elbow region in particle-laden flows. Increasing the turning radius of the pipeline elbow leads to a flatter flow field, decreased maximum velocity, and reduced velocity and pressure gradients within the elbow. The maximum velocity is consistently located on the inner wall of the bend, with particle motion trajectories shifting towards the outer side of the pipeline. As the turning radius increases, the

erosion area of particles decreases, but the overall erosion rate increases.

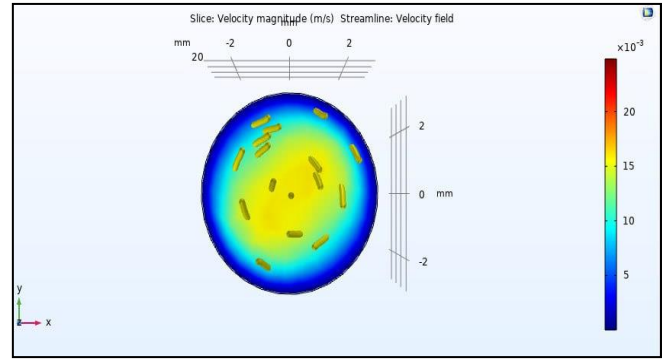


Figure 9. Erosive wear rate [kg/m².sec] on pipe walls, which had been modeled by utilizing Finnie model

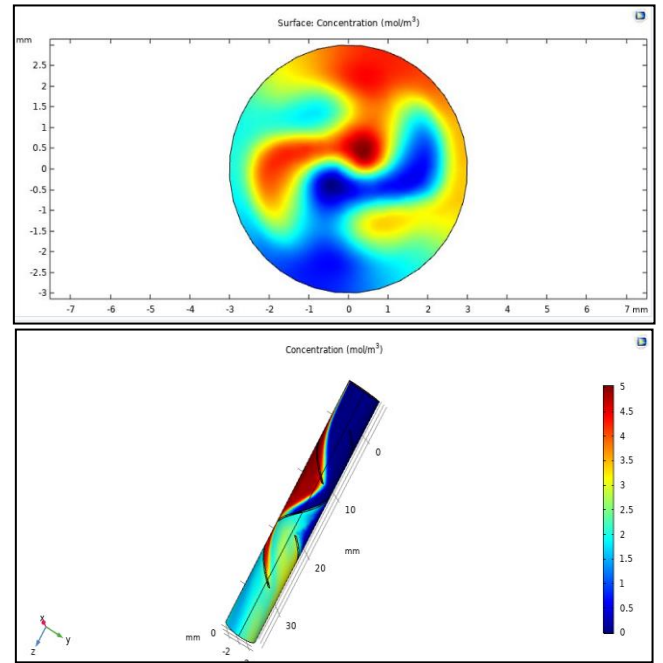


Figure 10. Erosive wear rate [kg/m².sec] on pipe walls, modeled with the use of ECRC model

The model is used for the evaluation of the single and two-phase flows. While the experimental tests were performed at low mass loading, sufficient level of four-way coupling is presumed as soon as the inter-particle collisions may be significant for the cases connected with the twisted pipe wall. In the present approach, as compared with other CFD methods applied to the analysis of MPLs, both inter-particle collisions and particles themselves do influence the overall fluid flow. The solution procedure is summarized as follows: first to calculate the single phase flow solution of the pipe. Then, the computed solution is employed for predicting the motion of the particles with a focus on the mentioned computational domain. In this case the phase to phase momentum exchange is calculated in every time step of the fractional steps process. At particle-wall boundary, in specific region of pipe wall all the required parameters like angle of incidence, velocity, frequency etc are recorded at each computational cell.

Finnie erosion models exhibited maximum corrosion wear rates of 6.13×10^{-10} kg/(m².s) and 1.91×10^{-10} kg/(m².s), whereas E/CRC erosion models had a maximum corrosion wear rate of

$9.03 \times 10^{-11} \text{ kg}/(\text{m}^2 \cdot \text{s})$. The comparison shows that the E/CRC model has the lowest maximum corrosion rate when compared to the preceding two. Figure 7 illustrates a pressure contour map. The pressure contour map indicates that at the elbow, the pressure on the outside of the pipe is greater than the pressure on the inside. Most fluids change direction due to centrifugal force. Because of the fluid's deposition, the pressure on the exterior wall is higher than that on the inside. The image demonstrates that internal pressure is negative, whereas elbow pressure increases from the inside out, as indicated in Figure 7. When the fluid enters the straight segment, its concentrated velocity peaks. Figure 6 shows how a fluid's flow direction changes when it passes over a pipe bend. When added to the velocity profile, the distribution of velocity changes, as seen in Figure 9. When an initial straight pipe section approaches the elbow point, the velocity of the entire pipe rises. As the fluid travels further along the pipe, it experiences separation phenomena. The flow direction changes as the elbow enters the second straight pipe section. Centrifugal force and gravity have a simultaneous effect on the flow distribution of velocity. At the time, the rate of change on the outside of the pipe is faster than on the interior. Despite the significant challenges caused by the synergistic impact of erosion-corrosion, the elbow's erosion-corrosion process, as driven by velocity and pressure, remains poorly understood because of its complexity. Numerical simulations play an important role in investigating the cases of erosion and corrosion. The higher velocity divergence on the four edges at the lower left intake coating is the result of the stronger wall lift force. Turbulent core area and boundary layer flow field of the fluid have a quite dissimilar context and that is why there is a decrease in the speed steadily in the first straight section. The layer of boundary possesses a blocking advantage to the movement of the fluid. The velocity gradient of each air parameter is high with the result of lift and proper flow. On the other hand, because of the unevenness and the disturbances on the elbows' edges, speed of the four vertices of a rotating dodecahedron changes.

The data used in the paper includes the size of the L-shaped pipeline, the opening degree of the flow control valve, the pressure at the starting point of the pipeline, and the mass of fluid flowing through the pipeline. The method includes: acquiring the size of an L-shaped pipeline; acquiring the opening degree of a flow control helical fin on the L-shaped pipeline in an helical fin operation process, the pressure of a starting point of the L-shaped pipeline in the helical fin operation process and the mass of fluid flowing through the L-shaped pipeline in the operation process, wherein the i is greater than or equal to 1; determining a computational formula of the maximum erosion rate of the size of the L-shaped pipe; and determining the maximum erosion rate of the L-shaped pipe according to the opening degree of the flow control valve on the L-shaped pipeline in the i -th operation process, the pressure of the starting point of the L-shaped pipeline in the i -th operation process and the mass of the fluid flowing through the L-shaped pipeline in the i -th operation process. The problem that the accuracy of the acquired maximum erosion rate of the L-shaped pipeline is low can be solved; the accuracy of the acquired maximum erosion rate of the L-shaped pipeline is improved; and the method and device can be used for determination of the maximum erosion rate of the L-shaped pipeline. The data on the size of the L-shaped pipeline, opening degree of the flow control valve, pressure at the starting point of the pipeline, and mass of fluid flowing

through the pipeline was chosen to determine the maximum erosion rate accurately. In the Figure 11, in this study, we examined the influence of wall shear on a pipe's behavior when containing diesel liquid, considering various elbow's different number of movement particle: (1 and 3 per inch) and velocities (10, 15, 20). The simulation was conducted using the CFD-software program. It is worth noting that the type of carbon particle remained constant throughout the study.

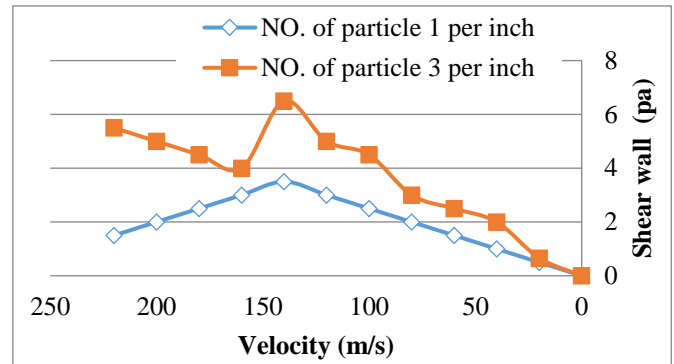


Figure 11. Relationship between velocity and wall shear with the different number of movement particle

In this paper, the outline about circular erosion test device for closed pipes is presented, where a fluid is whirled in a whirling device, then followed by delivering to the measuring device for measurement through the pipeline device. The open innovation file reveals the closed line circular erosion device. The circular erosion test device comprises a stirring device, a measuring device, a control device, a calibrating device and a pipeline device, wherein a medium is stirred in the stirring device, and then is conveyed to the measuring device for measuring through the pipeline device; the measuring device is connected with the control device; the control device is used for acquiring and adjusting the measurement data obtained by the measuring device; the calibrating device is connected with the measuring device and used for calibrating; the pipeline device comprises a stainless steel pipeline, and a to-be-tested pipeline which is a replaceable pipeline; the control device adopts a center console which comprises a data acquisition module, a temperature control module and a pressure control module. The circular erosion test machine contains the following benefits: it helps bring a comprehensive set of factors into the play, recreate the actual operating conditions, and provide a more accurate result.

The change in incidence acute angle is calculated by comparing the movement of pollution particles in the bend with varying intake velocity. The resulting acute angle of particles increases as input velocity increases, but the change range is limited and remains smaller than the initial acute angle of a straight pipe segment.

The important leakage sources are abrasion resulting from wear, localized corrosion, and turbulence/chemistry interactions. Corrosion, especially for metals and other materials, is a destructive and damaging process in an extensive number of engineering structures and components. Often pipe leaks or even pipe failures result from pipeline erosion and they both are dangerous and super expensive. The combination of corrosion and erosion creates synergy, where erosion increases corrosion rates with metal treatments that lead to preferential dissolving and vice versa. Excessive leakage is rarely an individual case of synergy between the

electrochemical corrosion and mechanical erosion. Its combination is generally responsible for a probability higher than the sum of these two causes alone. Additionally, elbows are the weakest links in social life and collection-transfer systems. In comparisons to destructive corrosion, erosion-corrosion research does not have a model yet that embraces impact of particle erosion, electrochemical corrosion, chemistry and fluid dynamics. The study area is chosen due to the remarkable importance of erosion-corrosion analysis in the process. Thus, the research is primarily devoted to the aspects of sample collection and analysis. Numerical modelling of the fluid flow, erosion and corrosion along the axial route of the pipeline for real-world cases and effects of the erosion-corrosion on the pipeline, the overall result would be the complete and realistic insight on erosion-corrosion failure.

The pressure fluctuation, as illustrated in Figure 7, is due to a geometric restriction that causes gases to build in the elbow section, and the accumulative effect puts comparatively high pressure on the extrados while considerably relieving pressure on the intrados.

9. CONCLUSION

1. In order to simulate the erosions, a 3D CFD model which describes turbulent transport of the particles of sand and oil via elbows was developed.

2. Particle tracking, turbulent modeling, and erosion simulation make up the comprehensive simulation model.

3. It has been determined that the proposed model has a potential to offer a better understanding of the complexity of the interacting and transporting processes, which are difficult to study experimentally.

4. The erosion-corrosion behaviors of elbows are simulated, and a model incorporating erosion, electrochemistry, corrosion, turbulence, and chemicals is developed to characterize the complex failure events. The findings are described below:

- a. Elbow erosion occurs around 40° and 50°, resulting in a sloping erosion region due to stress, boundary layer blockage, and wall rebound. Particles traveling at fast speeds collided with the tube's wall, particularly at the elbow portion, causing significant erosion on the elbow extrados.
- b. A particle count approach is presented to explain erosion and offer a probability estimate of elbow lifespan. Approximately 16.7% of particles impacted with the extrados area during erosion.
- c. The corrosion-causing current density of iron is concentrated at the junction of the straight section and elbow, as well as the point of intersection between the straight section and the elbow's intrados surface. The high turbulence intensity in the elbow and boundary layer impacts the concentration of chemical reactions that occur at the straight section-elbow junction.
- d. The pressure on extrados is greater than that on intrados. However, the friction velocity on the intrados is greater than that on the extrados, which is due to the cumulative impact of gas in the pipe. Low gas viscosity and geometric restrictions are thought to be responsible for the difference in magnitudes of velocity and particles striking the wall in a straight line.

REFERENCES

- [1] Abousnina, R.M., Manalo, A., Lokuge, W., Shiau, J. (2015). Oil contaminated sand: An emerging and sustainable construction material. *Procedia Engineering*, 118: 1119-1126. <https://doi.org/10.1016/j.proeng.2015.08.453>
- [2] Popoola, L.T., Grema, A.S., Latinwo, G.K., Gutti, B., Balogun, A.S. (2013). Corrosion problems during oil and gas production and its mitigation. *International Journal of Industrial Chemistry*, 4: 1-15. <https://doi.org/10.1186/2228-5547-4-35>
- [3] Sanni, S.E., Olawale, A.S., Adefila, S.S. (2015). Modeling of sand and crude oil flow in horizontal pipes during crude oil transportation. *Journal of Engineering*, 2015: 457860. <https://doi.org/10.1155/2015/457860>
- [4] Zhang, Y., Reuterfors, E.P., McLaury, B.S., Shirazi, S.A., Rybicki, E.F. (2007). Comparison of computed and measured particle velocities and erosion in water and air flows. *Wear*, 263(1-6): 330-338. <https://doi.org/10.1016/j.wear.2006.12.048>
- [5] Chen, X., McLaury, B.S., Shirazi, S.A. (2006). Numerical and experimental investigation of the relative erosion severity between plugged tees and elbows in dilute gas/solid two-phase flow. *Wear*, 261(7-8): 715-729. <https://doi.org/10.1016/j.wear.2006.01.022>
- [6] Al-Baghdadi, M.A., Resan, K.K., Al-Waily, M. (2017). CFD investigation of the erosion severity in 3D flow elbow during crude oil contaminated sand transportation. *Engineering and Technology Journal*, 35(9A), 930-935. <https://doi.org/10.30684/etj.35.9a.10>
- [7] Lafta, A.M., Jebuer, H.M., Obaid, M.A. (2023). Conduction and convection cooling of micro-chip device (electrophoresis device). *AIP Conference Proceedings* 2845(1): 070002. <https://doi.org/10.1063/5.0170414>
- [8] Mansour, M.M., Salman, H.S., Lafta, A.M., Nashee, S.R., Shkarah, A.J. (2024). Simulation analysis of protection oil pipe in platform to reduced corrosion and erosion defect with sustainability technique. *Mathematical Modelling of Engineering Problems*, 11(5): 1171-1178. <https://doi.org/10.18280/mmep.110505>
- [9] Homicz, G.F. (2004). Computational fluid dynamic simulations of pipe elbow flow (No. SAND2004-3467). Sandia National Laboratories (SNL), Albuquerque, NM, and Livermore, CA, United States.
- [10] Ahlert, K.R. (1994). Effects of particle impingement angle and surface wetting on solid particle erosion of AISI 1018 steel. Doctoral dissertation, BUiversity of Tulsa.
- [11] Duarte, C.A.R., de Souza, F.J., de Vasconcelos Salvo, R., dos Santos, V.F. (2017). The role of inter-particle collisions on elbow erosion. *International Journal of Multiphase Flow*, 89: 1-22. <https://doi.org/10.1016/j.ijmultiphaseflow.2016.10.001>
- [12] Bikbaev, F.A., Maksimenko, M.Z., Berezin, V.L., Krasnov, V.I., Zhilinskii, I. B. (1972). Wear on branches in pneumatic conveying ducting. *Chemical and Petroleum Engineering*, 8(5): 465-466.
- [13] Bikbaev, F.A., Krasnov, V.I., Maksimenko, M.Z., Berezin, V.L., Zhilinski, I.B., Otroshko, N.T. (1973). Main factors affecting gas abrasive wear of elbows in pneumatic conveying pipes. *Chemical and Petroleum Engineering*, 9(1): 73-75.
- [14] Amsden, A.A., Orourke, P.J., Butler, T.D. (1989).

- KIVA--II: A computer program for chemically reactive flows with sprays (No. LA-11560-MS). Los Alamos National Lab. (LANL), Los Alamos, NM, United States. <https://doi.org/10.2172/6228444>
- [15] Duarte, C.A.R., de Souza, F.J., dos Santos, V.F. (2015). Numerical investigation of mass loading effects on elbow erosion. *Powder Technology*, 283: 593-606. <https://doi.org/10.1016/j.powtec.2015.06.021>
- [16] Hashish, M. (1984). A modeling study of metal cutting with abrasive waterjets. *Journal of Engineering Materials and Technology*, 106(1): 88-100. <https://doi.org/10.1115/1.3225682>
- [17] Huang, C., Wells, L.K. Norton, L.D. (1999). Sediment transport capacity and erosion processes: Model concepts and reality. *Earth Surface Processes and Landforms: The Journal of the British Geomorphological Research Group*, 24(6): 503-516. [https://doi.org/10.1002/\(SICI\)1096-9837\(199906\)24:6<503::AID-ESP972>3.0.CO;2-T](https://doi.org/10.1002/(SICI)1096-9837(199906)24:6<503::AID-ESP972>3.0.CO;2-T)
- [18] Hamood, H.M., Mansour, M.M., Lafta, A.M., Nashee, S.R. (2023). Numerical investigation to study the effect of three heights of triangular obstacles on heat transfer of nanofluids in a microchannel. *International Review of Mechanical Engineering*, 17(11): 23627. <https://doi.org/10.15866/ireme.v17i11.23627>
- [19] Doos, Q.M., Mansour, M.M. (2018). Estimation of future thickness of carbon steel pipe and curing time of adhesive of GRE pipe by using neural network models. *Association of Arab Universities Journal of Engineering Sciences*, 25(5): 579-597.
- [20] Dawwod, L.M., Al-Kindi, L., Mansour, M.M. (2015). Analysis of maintenance activities in oil lubrication refinery using statistical techniques. *Engineering and Technology Journal*, 33(6A): 1494-1503. <https://doi.org/10.30684/etj.33.6A.18>
- [21] Mansour, M.M., Hamood, H.M., Lafta, A.M., Nashee, S.R., Shkarah, A.J. (2024). Enhancing the efficacy of adsorption-based carbon storage systems: A finite element analysis approach. *International Journal of Energy Production and Management*, 9(1): 19-24. <https://doi.org/10.18280/ijepm.090103>
- [22] Edwards, J.K., McLaury, B.S., Shirazi, S.A. (2001). Modeling solid particle erosion in elbows and plugged tees. *Journal of Energy Resources Technology*, 123(4): 277-284. <https://doi.org/10.1115/1.1413773>